Phase diagram of highly asymmetric binary mixtures: A study of the role of attractive forces from the effective one-component approach

J. Clément-Cottuz, S. Amokrane,* and C. Regnaut
Groupe de Physique des Milieux Denses, Faculté des Sciences et de Technologie, Université Paris XII Val de Marne, 61 Avenue du Général de Gaulle, 94010, Créteil Cedex, France
(Received 16 August 1999)

The phase diagram of an asymmetric solute-solvent mixture is investigated at the level of the effective one-component fluid. The solvent is taken into account by computing the potential of mean force between solute particles at infinite dilution for different models of solvent-solvent and solute-solvent short range interactions. Fluid-fluid and fluid-solid coexistence lines are determined from the free energy in the reference hypernetted chain theory for the fluid branch and from a variational perturbation theory for the solid one. The phase boundaries so determined compare well with recently published Monte Carlo data for mixtures of pure hard spheres. The influence of solute-solvent and solvent-solvent short range attractive forces is then investigated. When compared with pure hard core interactions, these forces are found to produce dramatic changes in the phase diagram, especially on the solvent packing fractions at which a dense fluid of solutes can be stable and on the separation of the fluid-fluid and fluid-solid coexistence lines. Finally, the connection of these results with the behavior of some colloidal suspensions is emphasized.

PACS number(s): 64.70.−p, 61.20.Gy, 82.70.−y

I. INTRODUCTION

The phase behavior of asymmetric binary mixtures of hard spheres has been the subject of an abundant literature in the past decade, in contrast with the case of mixtures with attractive forces. A fundamental interest of the former lies in the fact that when the hard sphere diameter ratio $R \equiv d_2/d_1$ is sufficiently high they may undergo a phase separation driven by purely repulsive forces (hereafter 1 and 2 refer to the small and large spheres, respectively). While the underlying mechanism or so called depletion effect was known from the early work on colloid-polymer mixtures [1,2] a new impetus has been given to these studies by the work of Biben and Hansen [3]. By using particular closures of the Ornstein-Zernike equations (OZE's), these authors indeed pointed out a possible phase separation in asymmetric mixtures of hard spheres. This result being in contradiction with the classical study by Lebowitz and Rowlinson [4] based on the Percus-Yevick (PY) closure, such mixtures have thus been studied by various methods ranging from the OZE's [5], density functional theory [6] (see also [7] for hard cubes), approaches based on the entropy [8], the free volume [9,10], the virial equation of state and virial expansions (see, for example, [11,12] and [13–15] and references therein) to computer simulations (see [16] for early work and [17–21] for more recent studies). In this last group, the recent study of Dijkstra *et al.* [19] has established that, in the effective one-component representation, the fluid-fluid transition is metastable with respect to the fluid-solid one.

Besides their intrinsic interest, these studies may be of more direct relevance to the interpretation of some experimental data. Indeed, a picture in terms of pure hard sphere mixtures is often invoked in order to explain the behavior of sterically stabilized suspensions in which the interactions are believed to be dominated by hard core repulsion [22–24]. It should be noted here that the depletion attraction invoked in these interpretations arises from the presence of smaller sized but otherwise supramolecular objects (added polymers, smaller sized solutes, etc.) but not from the solvent itself, which is viewed as an inert background (see, however, Ref. [25]). On the other hand, the effective interaction between solutes in pure solvent-colloid mixtures, that is, without such additional supramolecular species, has been found in several experiments to be strongly affected by several factors, up to the qualitative level. For instance, it was observed that changing the solvent [26] or the temperature [26,27] may turn it from effective attraction to effective repulsion. Various experiments have also shown that AOT-water in oil micelles exhibit a behavior that depends strongly on the nature of the oil [28–32]. The modification of the surface layer of sodium dodecyl sulfate (SDS) [33] or AOT [34] reverse micelles by a cosurfactant is now known to have a strong impact on the conductivity or intermicellar structure. The behavior of such a variety of physical systems, richer than that expected from purely steric effects, emphasizes again the competition between entropy and enthalpy, which is well known in the theory of ordinary mixtures.

From the theoretical point of view, studies based on Baxter's sticky hard sphere model [35] in the PY approximation have underlined the effect of short range attractions and in particular the crucial role played by heteroadhesions (see, for example, [36–40]). Recently, more realistic models of the interactions have been considered and their influence investigated at the level of the potential of mean force of solutes at infinite dilution both by analytical approaches [41–43] and by simulation [44]. These studies emphasized again the strong impact of attractive forces. The latter has in particular confirmed the qualitative predictions on the role of solute-solvent attractions at the level of the potential of mean force and the pair distribution function of the solute particles. The

*Author to whom correspondence should be addressed.

influence of such attractions on the phase diagram seems thus worth being considered in detail, since previous studies focused exclusively on structural properties. We have chosen to investigate this by means of the effective one-component representation of the mixture first because of the limitations of present theoretical methods. Indeed, no reliable integral equations of the reference hypernetted chain (RHNC) type exist for highly asymmetric mixtures, because of the lack of appropriate bridge functions (see, for example, the comparison of different closures in Ref. [41] and the discussion of the HNC Padé approximation of Attard and Patey [45], who attempted to compute the bridge functions in the high asymmetry regime). The situation is not easier if one attempts to study the real mixture by simulation. Indeed, a study of the kind of that presented by Dijkstra *et al.* [19] for a pure hard sphere mixture would be prohibitive in the presence of attractions. In addition to the common difficulties in sampling solute configurations, one should then compute the change in energy for configurations involving several thousands of small particles (and possibly a few hundreds of large ones). Finally, one important result of that study is the fact that the fluid-solid (F-S) coexistence line obtained from the simulation of the true mixture is not very different from that of the effective fluid. The situation is less clear for the fluid-fluid (F-F) line, the much higher effective packing fractions η_1^* of the small spheres then involved prohibiting direct simulation of the mixture (see, however, [20]). The good agreement between both types of simulations at low η_1^* (see also Ref. [17] for a similar observation on the pair distribution function of large spheres) suggests that the effective fluid representation of the kind adopted here should be adequate, at least for stressing the qualitative changes introduced by attractive forces in the phase diagram at high size asymmetry. As specified above, this aspect is indeed the main objective of this work.

This paper is organized as follows: In Sec. II, the theoretical tools required to compute the phase diagram are briefly presented. They are tested against simulation data for hard sphere mixtures in Sec. III. Finally, results with attractive forces are presented in Sec. IV.

II. THEORETICAL BACKGROUND

A. Potential of mean force for solutes at infinite dilution

The description of asymmetric mixtures at the effective one-component or McMillan-Mayer level is based on the potential of mean force at infinite dilution of the solutes and fixed solvent chemical potential μ_1 [46]. It can also be defined by formally integrating over the solvent degrees of freedom (see, for example, [17] and [19]). For practical applications of this formalism one usually neglects the many body nature of this potential, and assumes it as pairwise additive. The study of the mixture is thus reduced to that of a one-component fluid of solute particles interacting with an effective pair potential $\phi^{\text{eff}}(r)$, which reads (assuming interactions with spherical symmetry)

$$\phi^{\text{eff}}(r)=u_{22}(r)+\phi^{\text{ind}}(r), \tag{1}$$

where $u_{22}(r)$ is the direct solute-solute interaction potential and $\phi^{\text{ind}}(r)$ that between two solute particles induced by the solvent sea at chemical potential μ_1. In this work we used two methods for estimating $\phi^{\text{ind}}(r)$. In the first one the superposition approximation is used for the distribution function of the solvent about two isolated solutes (see, for example, [17,43,47]). The mean force between two spheres can then be expressed as [43]

$$F(r)=\frac{\pi}{r^2}\rho_1^b\int_0^\infty dr'\frac{\partial}{\partial r'}u_{12}(r')g_{12}(r') \times\int_{|r-r'|}^{r+r'}du\,u(r^2+r'^2-u^2)h_{12}(u), \tag{2a}$$

where $u_{12}(r)$ is the solute-solvent interaction potential, $g_{12}(r)=1+h_{12}(r)$ the associated pair distribution function, and ρ_1^b the solvent bulk density ($\eta_1^*=\pi\rho_1^b d_1^3/6$ is the solvent bulk packing fraction). As in Ref. [17], $g_{12}(r,\rho_2\to 0)$ was computed from the analytical solution of the PY closure of the OZE. The solvent induced potential of mean force $\phi^{\text{ind}}(r)$ is then obtained by numerical integration,

$$\phi^{\text{ind}}(r)=\int_r^\infty F(x)dx. \tag{2b}$$

In the second route, $\phi^{\text{ind}}(r)$ is directly computed from the pair distribution function of solutes at infinite dilution: $g_{22}(r;\rho_2\to 0)=\exp\{-\beta[u_{22}(r)+\phi^{\text{ind}}(r)]\}$ ($\beta\equiv 1/k_BT$). The OZE at infinite dilution,

$$\gamma_{11}(r)=\rho_1\int d\vec{r}\,'h_{11}(r')c_{11}(|r-r'|), \tag{3a}$$

$$\gamma_{22}(r)=\rho_1\int d\vec{r}\,'h_{12}(r')c_{12}(|r-r'|), \tag{3b}$$

$$\gamma_{12}(r)=\rho_1\int d\vec{r}\,'h_{11}(r')c_{12}(|r-r'|), \tag{3c}$$

must be supplemented by three closures, $g_{ij}=\exp(-\beta u_{ij}+\gamma_{ij}+B_{ij})$, where $\gamma_{ij}(r)=h_{ij}(r)-c_{ij}(r)$ and $B_{ij}(r)$ are the series and bridge functions, respectively. As noticed in the introduction, a reliable determination of $B_{ij}(r)$ is still difficult. The simplest alternative is to neglect these quantities altogether: $B_{22}(r)=B_{11}(r)=B_{12}(r)=0$. Mixed closures with not all $B_{ij}(r)$ equal to zero do not guarantee better results (see, for example, Ref. [41] for the potential and [48] for the structure of hard spheres at a wall). $\gamma_{22}(r)$ being given by Eq. (3b), we thus have in this HNC type of calculation

$$\beta\phi_{\text{HNC}}^{\text{ind}}(r)=-\gamma_{22}(r). \tag{4}$$

The potential of mean force from Eq. (2b) or Eq. (4) is the main input in the computation of the free energy of the effective fluid described below [that computed from Eq. (2) being of course much faster to evaluate]. The pertinent variables are then the chemical potential μ_1 of the solvent particles, the size ratio R, and the packing fraction $\eta_2=\pi\rho_2 d_2^3/6$ of the large spheres. Since there is no ambiguity in this effective one-component description, we will adopt in

the next section the notation $\eta \equiv \eta_2$ and $\rho \equiv \rho_2$. It will also be more practical to use the bulk packing fraction η_1^* instead of μ_1.

B. Pair structure and free energy in the RHNC theory

Among the various modifications of the HNC equation (generically denoted as MHNC), the RHNC theory with optimized reference system [49–51] is one of the most accurate integral equation methods for computing structural and thermodynamic properties of simple fluids (for recent applications see, for example, [52] for Lennard-Jones fluids and [53] for the Yukawa fluid). This is a well known method and we briefly recall here the main points. For an interaction potential $\phi(r)$ (one-component case), the optimized RHNC theory consists of the OZE,

$$\gamma(r) = \rho \int d\vec{r}\,' h(r') c(|r - r'|), \tag{5}$$

the closure,

$$g(r) = \exp\{-\beta\phi(r) + \gamma(r) + B_0(r)\}, \tag{6}$$

and the optimization condition, which for a hard sphere reference system reads

$$\int d\vec{r}\,[g(r) - g_0(r)] \frac{\partial}{\partial \sigma} B_0(r;\sigma) = 0. \tag{7}$$

In Eqs. (6) and (7) one utilizes the bridge function $B_0(r)$ for the hard sphere reference system whose pair distribution function $g_0(r)$, assumed known, depends on the hard sphere diameter σ. Equation (7) then determines the optimum σ ensuring a minimum free energy and when iterated until convergence together with Eqs. (5) and (6) the sought $g(r)$ for a given $\phi(r)$.

Our solution of Eqs. (5)–(7) is technically very similar to that detailed by Lomba [52]. We used the powerful algorithm of Labik *et al.* [54] based on a combination of the Newton-Raphson (NR) and successive substitution methods. For $B_0(r)$ we took the parametrization of Malijevski and Labik [55] including the region inside the hard core [56]. For the pair distribution function of the reference system $g_0(r)$, we used the PY solution with the Verlet and Weis correction [57]. In order to speed up calculations, the Kinoshita and Harada strategy [58] was found essential, as noted by Lomba [52]. In this strategy, the system matrix H (negative of the inverse of the Jacobian) computed under some reference condition is stored and used in other conditions. During the determination of the optimum σ or at a new density, for example, one computes the correction of the M Fourier components of $r\gamma(r)$, $\Delta\widetilde{\Gamma}_j = \Sigma_{k=1}^{M} H_{jk} \Psi_k$, without having to compute and invert the Jacobian in the inner NR loop. One nevertheless still faces the well known problem with integral equation methods, that is, the existence of a nonconvergence domain of the algorithm, in the temperature density plane (T,ρ). As discussed in the next section, this limitation will become especially severe with the effective potential $\phi^{\mathrm{eff}}(r)$ considered here.

Once the OZE with the RHNC closure is solved, the free energy is computed from the reference system free energy and integrals involving $g(r)$, $g_0(r)$, and the Fourier transforms $\tilde{h}(k)$ and $\tilde{h}_0(k)$ [Eqs. (10)–(15) in [51], recalled in the Appendix]. We notice here that in order to obtain a computable expression of the exact free energy (see the Appendix), the nonlocal contribution,

$$\beta \frac{\Delta A_3}{N} = -\frac{1}{2}\rho \int d\vec{r} \int_0^1 d\lambda\, B(r;\lambda) \frac{\partial}{\partial \lambda} g(r;\lambda), \tag{8}$$

is approximated by the local one,

$$\beta \frac{\Delta A_3}{N} \approx -\frac{1}{2}\rho \int d\vec{r}\, B_0(r)[g(r) - g_0(r)]. \tag{9}$$

In Eq. (8) $B(r;\lambda)$ and $g(r;\lambda)$ are the bridge and pair distribution functions for an interaction potential

$$\phi_\lambda(r) = \phi_0(r) + \lambda \phi_1(r), \tag{10}$$

where the charging parameter λ allows one to go from the reference system with interaction $\phi_0(r)$ to the fully interacting system with $\phi(r)$. Equation (9) follows from Eq. (8) by neglecting the change of $B(r;\lambda)$ from $\lambda = 0$ to $\lambda = 1$. Following Rosenfeld's discussion [59] of the MHNC theory, one can obtain a different approximation of the nonlocal term by considering the optimization condition [Eq. (7)] written for a given value λ of the charging parameter:

$$\int d\vec{r}\,[g(r;\lambda) - g_0(r)] \frac{\partial}{\partial \sigma(\lambda)} B_0(r;\sigma(\lambda)) = 0. \tag{11}$$

The optimum hard sphere diameter for the potential $\phi_\lambda(r)$ is then $\sigma(\lambda)$. Equation (11) can then be integrated by parts, giving

$$\beta \frac{\Delta A_3}{N} = -\frac{1}{2}\rho \int d\vec{r} \Big\{ B(r;1)g(r) - B(r;0)g_0(r) - \int_0^1 d\lambda\, g(r;\lambda) \frac{\partial}{\partial \lambda} B(r;\lambda) \Big\}. \tag{12}$$

By assuming that $B(r;\lambda)$ belongs to the family of hard sphere bridge functions $B(r;\lambda) = B_0(r;\lambda)$ and using $(\partial/\partial\lambda) B_0(r;\lambda) = (\partial/\partial\sigma) B_0(r;\sigma)(\partial\sigma/\partial\lambda)$ and Eq. (11), the last integral in Eq. (12) can be expressed entirely in terms of the reference system. The nonlocal term then reads

$$\beta \frac{\Delta A_3}{N} = -\frac{1}{2}\rho \int d\vec{r} \Big\{ B_0(r;1)g(r) - B_0(r;0)g_0(r) - \int_{\sigma(0)}^{\sigma(1)} d\sigma\, g_0(r;\sigma) \frac{\partial}{\partial \sigma} B_0(r;\sigma) \Big\}. \tag{13}$$

Since $B_0(r)$ is analytical and $g_0(r)$ can be computed by Fourier transform, the integral in Eq. (13) can be evaluated readily by numerical integration. This expression of the nonlocal term is analogous to that in Rosenfeld's treatment of the MHNC [59], except for the choice of the reference system. The difference between the free energies evaluated with expressions (9) and (13) of the nonlocal term should be a measure of the adequacy of the hard sphere bridge function

(and the universality assumption [60]) for the rather unusual interaction potential $\phi^{\text{eff}}(r)$ considered here.

The free energy can of course be evaluated only outside the nonconvergence domain. It will thus be useful to consider the alternative expression

$$\beta\frac{A}{N}=\beta\frac{A_0}{N}+\int_0^1 d\lambda\, U^{\text{ex}}(\lambda), \tag{14a}$$

where the energy integral U^{ex} computed from the excess interaction defined in Eq. (10) is evaluated for the value λ of the charging parameter

$$U^{\text{ex}}(\lambda)=\frac{1}{2}\rho\int d\vec{r}\, g(r;\lambda)\phi_1(r). \tag{14b}$$

Equation (14) is well known (see [61]) and has been used in an equivalent form by Dijkstra *et al.* [19] to compute the free energy by Monte Carlo (MC) simulation. Equations (14) will be used in the next section to estimate the free energy beyond the nonconvergence line.

We mention here that the coexistence lines were obtained from the common tangent instead of the direct Maxwell construction (equating the pressure and chemical potential of coexisting phases). Although the RHNC guarantees consistency between the virial pressure and that obtained by differentiating the free energy [50], numerical uncertainties in the evaluation of the virial pressure with very large values of $g(r)$ near contact together with the limitation due to the nonconvergence line make the former method more practical.

To end this section, we stress that the RHNC free energy is appropriate only to the fluid branch. The treatment of the solid one by variational perturbation theory (VPT) will be detailed in the next section.

III. BINARY MIXTURE OF HARD SPHERES

A. Pair distribution function

In this section, we present some results obtained from the formalism of the previous section for a binary mixture of hard spheres. In order to test the quality of the RHNC closure for this specific system, we first compared $g(r)$ computed with the ''depletion'' potential obtained by molecular dynamics (MD) by Biben *et al.* [17] with the result of the simulation of the effective fluid (state *A* in Ref. [17]: $R=10$, $\eta_1^*=0.106$, $\eta\equiv\eta_2=0.244$). The excellent agreement shown in Fig. 1(a) is not unusual for this rather moderate interaction [with well depth $\beta\phi^{\text{ind}}(d_2)\approx-1.62$]. Somewhat less expected is the fact that the RHNC can capture the fine structure induced near $r=d_2+d_1$ by the weak oscillation of $\phi^{\text{ind}}(r)$ (the amplitude of its first maximum is less than $0.15kT$). In contrast, the agreement is less good for a state point well inside the fluid-solid coexistence region [Fig. 2 with the depletion potential $\phi_{\text{dep}}(r)$ given by Eq. (33) in Ref. [19]]. In particular, the RHNC does not reproduce the first peak near $r=1.74d_2$ [Fig. 1(b)] despite its magnitude being larger than that near $r=d_2+d_1$ in Fig. 1(a). This is not really surprising since this ''extra'' peak might indeed be the signature of a partly solidlike $g(r)$. Finally, Fig. 1(c) again shows a good agreement [62] for a stronger depletion potential computed from Eqs. (2) (PY+superposition approxima-

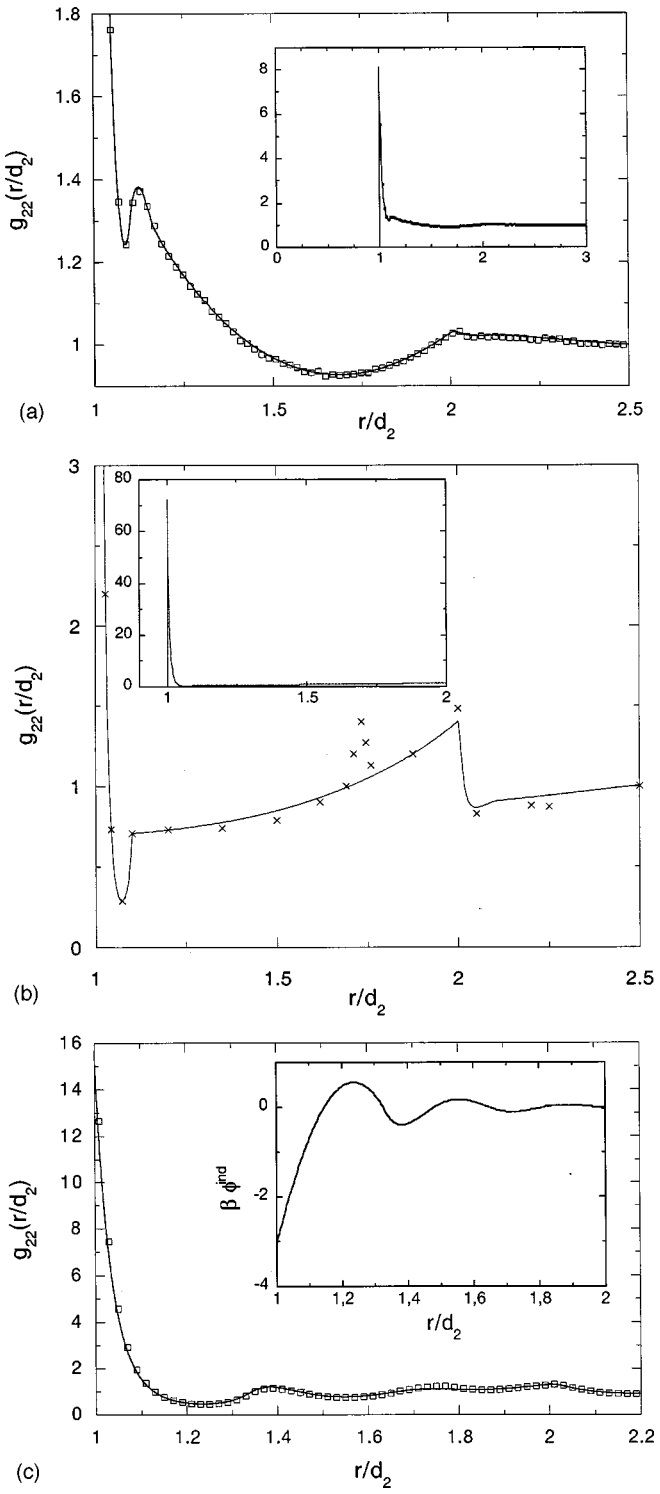

FIG. 1. (a) Pair distribution function $g_{22}(r)$ of large spheres with packing fraction $\eta_2=0.244$, for the depletion potential of Ref. [17] (diameter ratio $R=10$, small sphere bulk packing fraction $\eta_1^*=0.106$). Solid line: RHNC; squares: Monte Carlo [17] and private communication. (b) $g_{22}(r)$ at $\eta_2=0.35$ for the depletion potential ϕ_{dep} of Ref. [19] ($R=10$, $\eta_1^*=0.25$). Solid line: RHNC; crosses: Monte Carlo [19]. (c) $g_{22}(r)$ at $\eta_2=0.25$ for ϕ^{ind} ($R=3$, $\eta_1^*=0.37$). Solid line: RHNC; squares: Monte Carlo [62] [inset shows ϕ^{ind} computed from Eqs. (2)].

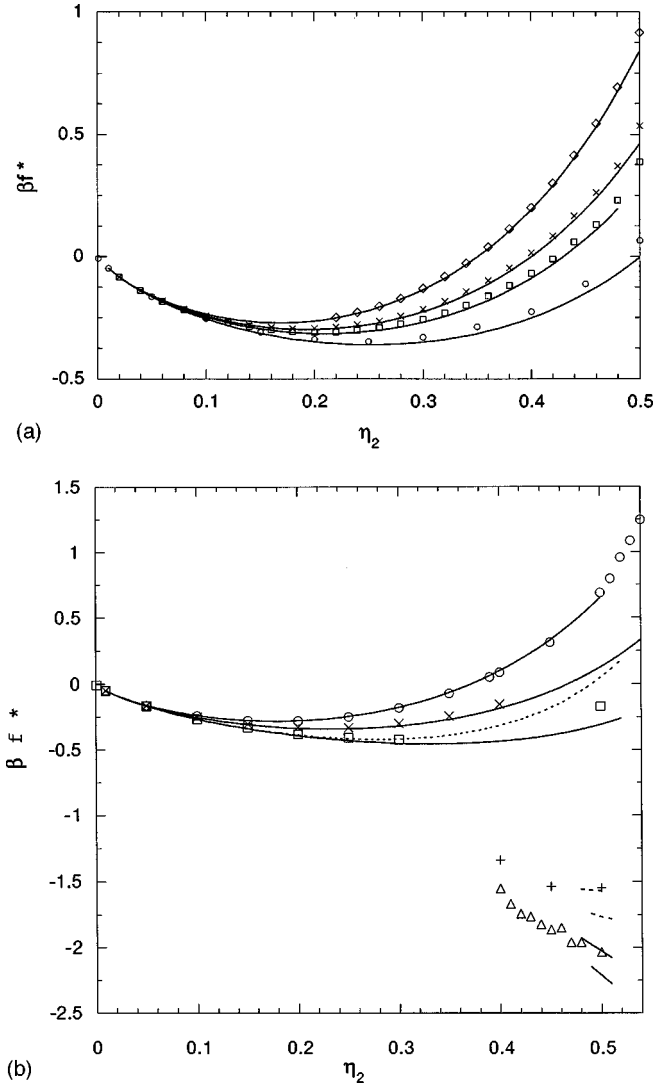

FIG. 2. (a) Iso-η_1^* reduced free energy $\beta f^* \equiv \beta(A/N)\eta_2$ vs η_2 at $R=5$. RHNC: solid lines; Monte Carlo [19] and private communication: diamonds $\eta_1^*=0.13$, crosses $\eta_1^*=0.21$, squares $\eta_1^*=0.24$, circles $\eta_1^*=0.30$. (b) Same as 3(a) with $R=10$. Solid lines: RHNC with Eq. (9); dashed lines: RHNC with Eq. (13). Monte Carlo data: circles $\eta_1^*=0.13$, crosses $\eta_1^*=0.17$, squares $\eta_1^*=0.20$, pluses $\eta_1^*=0.30$, triangles $\eta_1^*=0.31$ (the solid curves follow the same sequence and the dashed lines are for the last three values of η_1^*).

tion) for $R=3$, $\eta_1^*=0.37$, $\eta=0.25$. These results gave us some confidence in the structure obtained from the RHNC.

One technical point is worth mentioning here. In order to properly account for the variation of $\phi^{\text{ind}}(r)$ on a scale that is determined by the solvent diameter d_1, we need an appropriate mesh spacing. Taking $dr=0.02d_1$ means $dr=0.002d_2$ for $R=10$. Because of the constraint $dq\,dr=\pi/N_r$ imposed by the fast Fourier transform algorithm, the number of mesh points N_r required for a good resolution in reciprocal space can be very large. In some instances N_r had to be as large as 16 384 and $M\approx 256$ in the inner NR loop which involves (M,M) matrices. These conditions due to the very short range of $\phi^{\text{ind}}(r)$ (at the scale of the big spheres) illustrate one of the specificities of this effective potential when compared to more standard ones (e.g., the Lennard-Jones potential).

B. Free energy and fluid-fluid coexistence line

We next computed the RHNC free energy at constant η_1^* for the depletion potential $\phi_{\text{dep}}(r)$. Figure 2(a) shows the comparison of the reduced free energy with MC data [19] for $R=5$, and Fig. 2(b) for $R=10$. We first notice that at low η_1^* the agreement is excellent at all large sphere packing fractions η_2 but it deteriorates for higher η_1^* especially at high η_2. A noteworthy feature is that the free energies computed from Eq. (9) and from Eq. (13) of the nonlocal term $\beta\Delta A_3/N$ do not give the same results at high η_2. This discrepancy might be an indication of the insufficiency of the hard sphere bridge function for an effective potential of the kind of $\phi_{\text{dep}}(r)$, which is rather narrow and deep near contact. The comparison with present MC data does not allow us to say which expression should be preferred. As a rule, Eq. (9) for $\beta\Delta A_3/N$ would predict a lower critical value of η_1^* than Eq. (13). A more systematic discussion of this point is deferred to future work and in what follows, the results that will be discussed will correspond to Eq. (9).

Figure 2(b) now shows that beyond a certain value of η_1^*, one faces the problem of nonconvergence (NC) of the algorithm. As discussed elsewhere [63–65], this is an intrinsic feature of HNC type integral equations and not the signature of a physical instability such as a spinodal one. This problem, which constitutes a major drawback of such methods, is here especially severe. Direct determination of the coexisting densities indeed revealed it to be impossible, the metastable and unstable parts of the free energy being always in the NC domain (η_1^*,η_2) at all the diameter ratios we investigated. We were then forced to devise an *ad hoc* extrapolation procedure in order to estimate the free energy inside the NC domain. This extrapolation is based on Eqs. (14) for the free energy. We mention here that the free energy computed by this method was numerically consistent with the RHNC free energy computed with Eq. (9) (see Ref. [50] for the role of the optimization criterion). A small inconsistency was found when Eq. (13) was used instead of Eq. (9). By computing the energy integral $U^{\text{ex}}(\lambda)$ in Eq. (14b) for values of λ increasing from 0 to 1, we reach a certain value λ_{NC} beyond which the algorithm fails to converge. This value is specific to each couple (η_1^*,η_2) but was never found below $\lambda_{\text{NC}}\approx 0.85$. In order to estimate the actual free energy $(\lambda=1)$, we then had to extrapolate $U^{\text{ex}}(\lambda)$ over a small range. This was shown to be finally equivalent to directly performing a polynomial extrapolation of the integral [Eq. (14a)] to $\lambda=1$. By changing the degree of the polynomial (Fig. 3) we found that the densities at coexistence are not very sensitive to the extrapolation procedure. Outside the NC domain it is also possible to compare the extrapolated values with the directly computed ones. As an additional test, the gas and liquid coexistence densities (η_2^g,η_2^l) were checked against a Maxwell construction made by directly extrapolating the virial pressure $P(\eta_2)$ in the NC domain. This much more drastic density extrapolation gave similar coexistence densities for the cases we have tested. With $R=10$ and $\eta_1^*=0.262$, for example, these densities were $(0.22, 0.51)$ with the λ extrapolation

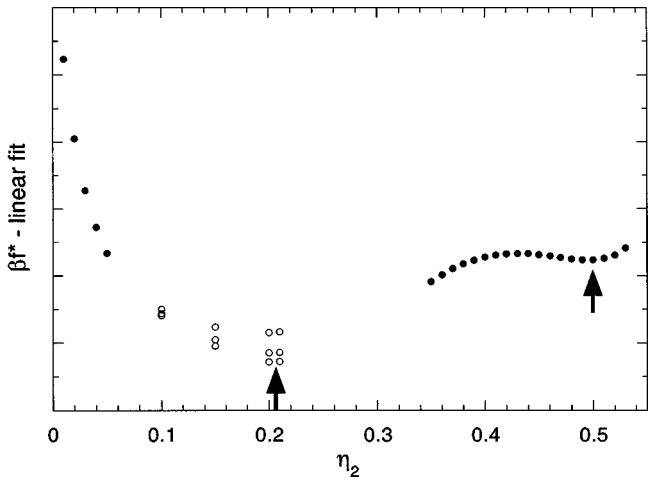

FIG. 3. RHNC reduced free energy (minus a linear fit) for $\phi_{\rm dep}$ ($R=10$, $\eta_1^*=0.262$). Filled circles: direct result ($\lambda=1$). Empty circles: extrapolation to $\lambda=1$ with polynomials of degree 4, 6, and 8 from top to bottom. The arrows indicate the locations of the common tangent.

method and (0.21, 0.50) with the $P(\eta_2)$ one. These satisfactory tests gave us some confidence in this method of estimating the F-F coexistence line. It must be mentioned, however, that this procedure is rather lengthy, since the optimized RHNC must be solved for a series of values of λ, for each set of (η_1^*,η_2), besides the required checks of the sensitivity to the extrapolation procedure. Thus it cannot be used in a routine way.

Figure 4(a) then shows on an enlarged scale the estimated RHNC F-F coexistence lines and that determined by MC simulation [19]. This figure shows that the RHNC lines [free energies from Eq. (9) and Eq. (13) for $\beta\Delta A_3/N$] ''bracket'' the simulation one. Given the uncertainties in the theory, this is a rather positive observation. On the other hand, the upward rise of the simulation curve for $\eta_2\geqslant 0.45$ in the (η_1,η_2) representation in Fig. 4(b) is not reproduced by the theory [the conversion $(\eta_1^*,\eta_2)\rightarrow(\eta_1,\eta_2)$ was made by using the scaled particle theory expression of η_1^*]. We found a similar behavior on the PY-compressibility coexistence line [66] of the sticky hard sphere model mapped onto $\phi_{\rm dep}(r)$. The stickiness parameter τ was converted into η_1^* by equating the second virial coefficients of the sticky potential and that of $\phi_{\rm dep}(r)$ (these quantities do not, however, strictly play the same role). A similar observation [67] holds when the free energy is determined from integration of the virial equation of state as in Ref. [11]. Whether this is due to the theoretical free energies being inadequate for highly packed metastable fluids is at present unclear to us.

Finally, we found it interesting to investigate the influence of truncating the depletion potential. In Ref. [19] it was conjectured that this should have a minor influence on the phase boundaries, starting from a comparison of the $g(r)$ determined with and without the oscillations in $\phi_{\rm dep}(r)$ beyond the second zero. In order to estimate the effect of such oscillations we computed several iso-η_1^* virial pressure curves with the effective potential $\phi^{\rm ind}(r)$ from Eqs. (2). The example shown in Fig. 5 ($R=5$, $\eta_1^*=0.32$) shows that the overall effect of the oscillations is to decrease the pressure, the full potential being more ''attractive'' than the one truncated after the second zero. Because of the time required to perform the λ extrapolation procedure, we did not make a systematic estimation of the coexistence line for such potentials but we expect the corresponding critical point in the (η_1^*,η_2) representation to be lower than that with the truncated potential.

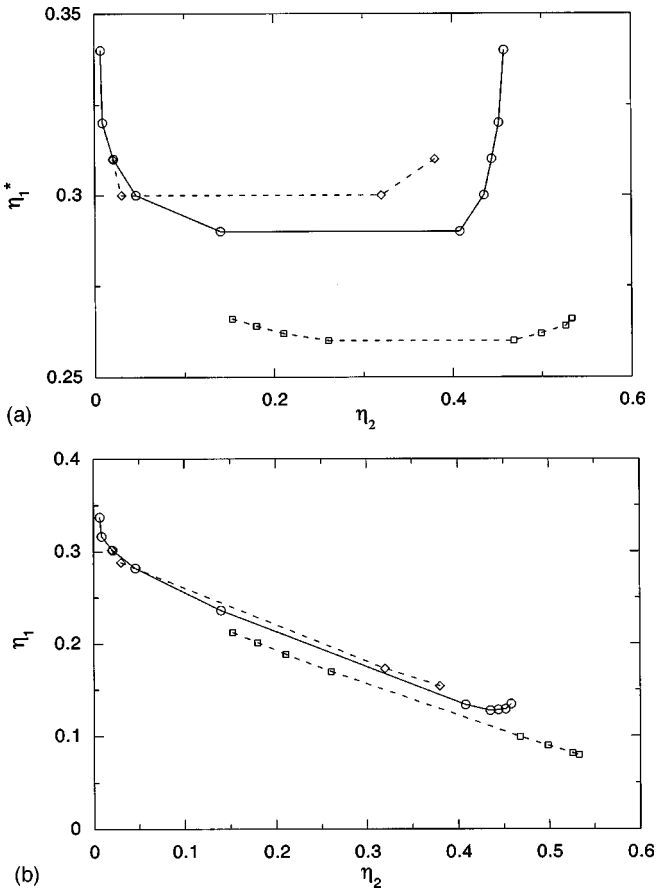

FIG. 4. (a) Fluid-fluid coexistence line in the η_1^*-η_2 representation. Diamonds: RHNC with Eq. (13); squares: RHNC with Eq. (9); circles: Monte Carlo [19]. (b) Same as 4(a) in the η_1-η_2 representation.

C. Fluid-solid branch

To complete the phase diagram, the fluid-solid (F-S) boundary must be determined. As mentioned at the end of Sec. II, a theory for homogeneous fluids as the RHNC cannot deal with the solid phase. We nevertheless tried the entropy criterion of Giaquinta and Giunta [68] but very few zeros of the residual entropy can actually be determined because of the NC limitation (the λ extrapolation is useless in this case). It is difficult to draw firm conclusions from the points shown in Fig. 6(a) but the line of zero residual entropy is likely to be below the RHNC F-F line but much above the F-S line from simulation.

We are thus presently investigating the determination of the F-S line from the density functional theory (see, for example, [69,70] and references therein). As a first estimate we used a much simpler route based on the well known variational perturbation theory expression of the free energy [61]:

$$A(\rho)=A_{\rm HS}(\rho)+\langle\phi-\phi_{\rm HS}\rangle_{\rm HS} \qquad (15)$$

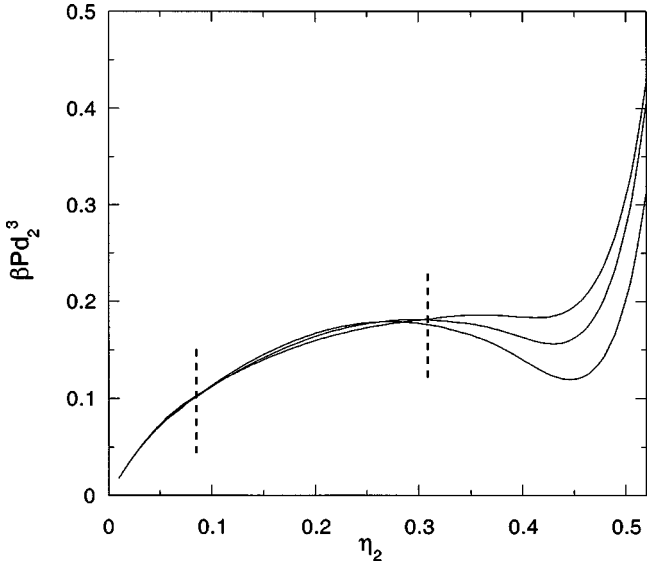

FIG. 5. Influence of the truncation of the effective potential on the pressure. ϕ^{ind} from Eqs. (2) with $R=5$ and $\eta_1^*=0.32$. From top to bottom: well plus first barrier; full potential, first well only (the parts of the curves in the nonconvergence domain delimited by the vertical lines were obtained from a cubic spline).

where the optimum hard sphere diameter σ^{opt} was obtained by minimizing $A(\rho)$. The technical details of our calculation, in particular the parametrization of the radial distribution function $\overline{g}_{\text{HS}}(r)$ for the solid, were identical to those in the study by Hasegawa [71] of the Yukawa potential. With ϕ_{dep}, the value of σ^{opt} minimizing $A(\rho)$ is always equal to d_2 and the method reduces to a perturbation calculation. However, no F-F line could be determined from the VPT with ϕ_{dep}, the free energy curves being supercritical even for $\eta_1^*=0.35$. Since the actual $g(r)$ for the liquid is very different from $g_{\text{HS}}(r)$, especially near contact, the perturbation treatment is strongly in error. We thus applied the VPT only to the solid, for which the true $\overline{g}(r)$ should not differ much from $\overline{g}_{\text{HS}}(r)$, especially at high η_2 and with a short range interaction such as ϕ_{dep} (see also the discussion in Ref. [72]). For the fluid branch we used instead the RHNC free energy, which indeed yields a F-F line.

As shown in Fig. 6(b), the region of the sharp minimum of the solid branch is indeed remarkably well reproduced by the VPT for the solid. The large discrepancies at high η_1^* and for η_2 below the position of the minimum do not affect the common tangent construction with the fluid branch. At the scale required to draw this tangent, using the RHNC values or the MC ones has no sizable effect (see the crosses near $\eta_2=0.5$ where the discrepancy is the largest). For η_1^* below 0.1, however, the solid boundary moves to lower values of η_2. The solid being then less densely packed, the influence of ϕ_{dep} on $\overline{g}(r)$ might become significant. But since the magnitude of ϕ_{dep} is then lower (and the perturbation term accordingly), the VPT still remains accurate. As a test, we took $\eta_1^*=0.05$, which corresponds to an abrupt change of the slope of the MC solid branch. We then found ($\eta_2^f=0.50$, $\eta_2^s=0.59$) whereas the MC values are ($\eta_2^f=0.487$, $\eta_2^s=0.574$). The F-S line determined from the VPT for the solid and the RHNC (or MC) data for the fluid is then nearly identical to that using simulation data for both sides. This

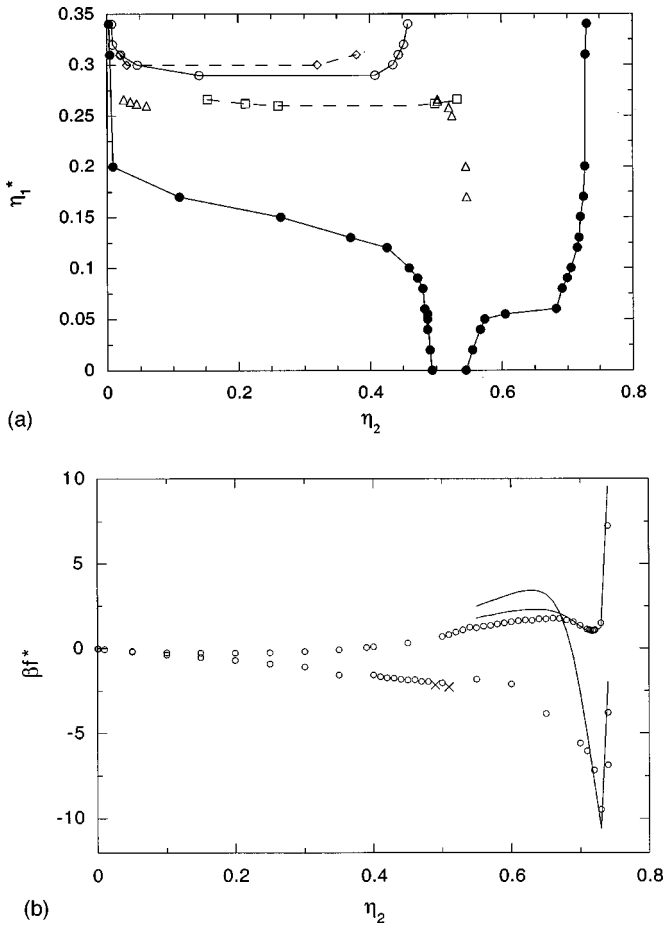

FIG. 6. (a) Fluid-fluid and fluid-solid coexistence lines of the binary hard sphere mixture ($R=10$). Diamonds: RHNC F-F line with Eq. (13): squares RHNC with Eq. (9); triangles: points of zero residual entropy; circles: Monte Carlo [19]. The hybrid RHNC-VPT F-S line (not shown) would almost coincide with the MC one. (b) Iso-η_1^* reduced free energies vs. η_2 for $R=10$. Full curves: VPT solid branch; crosses: RHNC fluid branch; circles: Monte Carlo [19]. Upper data: $\eta_1^*=0.13$; lower data: $\eta_1^*=0.31$.

hybrid RHNC-VPT method should then provide a reliable estimate of the F-S boundary, especially for the less deep potentials of the next section.

To summarize this section, we may say that the RHNC theory gives a good description of the structure of the effective fluid, representing a highly asymmetric binary mixture despite the fact that the effective potential is rather remote from that in the reference hard sphere system. The differences in free energies observed when two expressions of the nonlocal term are used might be the signature of the limitation of this reference system bridge function. This term is indeed the one involving an explicit contribution of the bridge function. To assess this point, we are presently investigating an alternative route using Rosenfeld's density functional theory [73]. Finally, and despite the *ad hoc* procedure used to estimate the free energy in the nonconvergence region and the hybrid construction of the F-S boundary, the positive comparison with simulation data led us to use this approach to investigate the role of attractive forces. From the numerical point of view, this situation is actually easier than that prevailing in hard sphere mixtures, as will be seen below.

IV. PHASE BOUNDARIES OF THE EFFECTIVE FLUID IN THE PRESENCE OF ATTRACTIVE FORCES

As stressed in the Introduction, studies of the role of attractive forces in the highly asymmetric regime are rather scarce and concerned mainly with structural properties or the potential of mean force. The present work is, to our knowledge, the first one to report results on the phase diagram in this regime (see [74] for nonadditive hard spheres). Since we are interested in the role of attractions, repulsive forces will not be discussed here (we may quote the study in [75] on a mixture of hard spheres and repulsive Yukawa small spheres). A systematic study will not be attempted, the main objective being to show from some selected cases how these forces may alter the rather ''universal'' picture associated with pure hard core interactions. Indeed, one may then wonder how a variety of highly asymmetric colloidal suspensions may exhibit stable and dense fluid phases. We will thus start from the general observation [36–44] that attractions between unlike particles usually favor the dispersed state (one may roughly say that they lower the energetic contribution to the free energy). On the other hand, they give rise to a strongly oscillating but still short range induced potential [43]. Since short range is expected to be less favorable to a stable dense fluid, the most favorable situation should be a not too deep and relatively long range $\phi^{\mathrm{ind}}(r)$. The first requirement can be achieved by adding an attractive tail to the interaction potential $u_{12}(r)$ and the second one by considering solvent particles with attractions [43]. We thus considered the 12-6 Lennard-Jones potential for u_{11}:

$$\beta u_{11}(r)=4\varepsilon_{11}^{*}\left\{\left(\frac{d_1}{r}\right)^{12}-\left(\frac{d_1}{r}\right)^{6}\right\}, \tag{16}$$

and a Yukawa form for u_{12}:

$$\beta u_{12}(r)=\begin{cases}\infty & r\leqslant d_{12}\\ -\varepsilon_{12}^{*}\exp[-\kappa(r/d_{12}-1)]/r & r>d_{12}\end{cases}. \tag{17}$$

In Eq. (16) the unlike spheres hard core diameter was taken as $d_{12}=(d_2+d^{\mathrm{eff}})/2$ where the ''effective'' hard core diameter of the Lennard-Jones potential was taken such that $u_{11}(d^{\mathrm{eff}})\approx 1.5\,kT$ (other choices could be considered as well).

The effective potential $\phi_{\mathrm{HNC}}^{\mathrm{ind}}(r)$ computed from Eq. (4) is shown in Fig. 7 for some values of ε_{12}^{*} and ε_{11}^{*}. When compared to the pure hard sphere case, the most prominent features of this effective potential are indeed the desired ones: (i) a strong reduction of the well depth at contact and (ii) the appearance of an attractive tail extending up to about $5d_1$ from contact, in agreement with the general discussion presented in Ref. [43]. In the absence of a direct comparison with simulation, it is difficult to know to what extent this is quantitatively correct but we have checked that these gross trends remain the same when $\phi^{\mathrm{ind}}(r)$ is computed as in Ref. [43] (see also [41,42] for similar considerations). This is sufficient for our present purpose.

We next determined the F-F and F-S boundaries by using the same method as for pure hard spheres. As mentioned in the previous section, the situation was easier from the numerical point of view. The extent of the nonconvergence domain being much smaller than in the case of hard spheres,

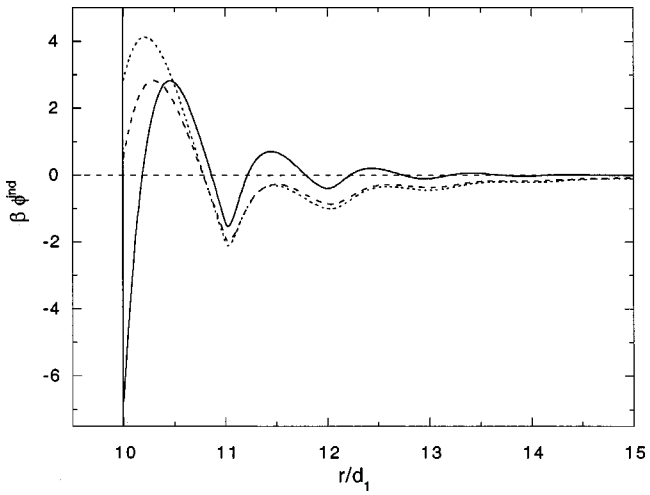

FIG. 7. Effective potential $\phi^{\mathrm{ind}}(r)$ with LJ solvent-solvent and Yukawa solute-solvent interactions from Eqs. (4), (6), and (17) and with $R=10$ and $\eta_1^{*}=0.366$. Solid line: pure hard sphere mixture; dotted line. $\varepsilon_{11}^{*}=0.6$, $\varepsilon_{12}^{*}=10$, $\kappa=2.5$; dashed line: $\varepsilon_{11}^{*}=0.5$, $\varepsilon_{12}^{*}=8$, $\kappa=2.5$.

direct (i.e., without λ extrapolation) determination of the F-F boundary was indeed often possible. The F-F lines with attraction [an example is shown in Fig. 8(a)] occur at much higher values of η_1^{*} than with pure hard spheres. Higher values are indeed necessary to produce enough attraction, since at the same η_1^{*}, the effective potential is naturally less deep than with pure hard spheres. Such high values of η_1^{*} correspond now to densities appropriate for bulk liquid solvents. This is in strong contrast with the observation [19] that for hard sphere mixtures, the value of η_2^{f} at coexistence is very low when η_1^{*} is high.

Besides this important observation that a dense fluid can exist even at high η_1^{*}, one important point is the position of the F-F line with respect to the F-S one. Several studies [71], [76,77] have shown that with standard interactions, the relative distance [in the (T,ρ) plane] between these boundaries changes with the interaction range, the F-F transition being stable with respect to the F-S one for sufficiently long attraction range. From the shape of $\phi^{\mathrm{ind}}(r)$ shown in Fig. 7, we expect a similar trend. Figure 8(a) shows that the F-S line is now close to the F-F one, although still below it. This suggests that $\phi^{\mathrm{ind}}(r)$ is still not long enough ranged (besides possible complications with oscillatory potentials). The gap between these lines is subject to the uncertainty in the determination of the F-F line [recall the discussion of Fig. 4(a)] but is much reduced when compared with that for pure hard spheres [19]. It is also to be noted that the F-S coexistence domain is also much narrower. At high η_1^{*}, the solid side boundary is almost a straight line near $\eta_2^{s}\approx 0.55$, far from that for pure hard spheres. This is a consequence of the fact that σ^{opt} is greater than the actual hard core diameter d_2 of $\phi^{\mathrm{ind}}(r)$. In Fig. 8(b), the optimized free energy of the solid branch (for $\eta_1^{*}=0.419$) is compared with that computed by taking $\sigma^{\mathrm{opt}}=d_2$ [this last value corresponds to a secondary and less deep minimum of $A(\rho)$]. The nonoptimized one is of course higher and shows a minimum at $\eta_2\approx 0.73$, a value close to the solid boundary for hard spheres. However, the construction of the common tangent with the fluid branch is

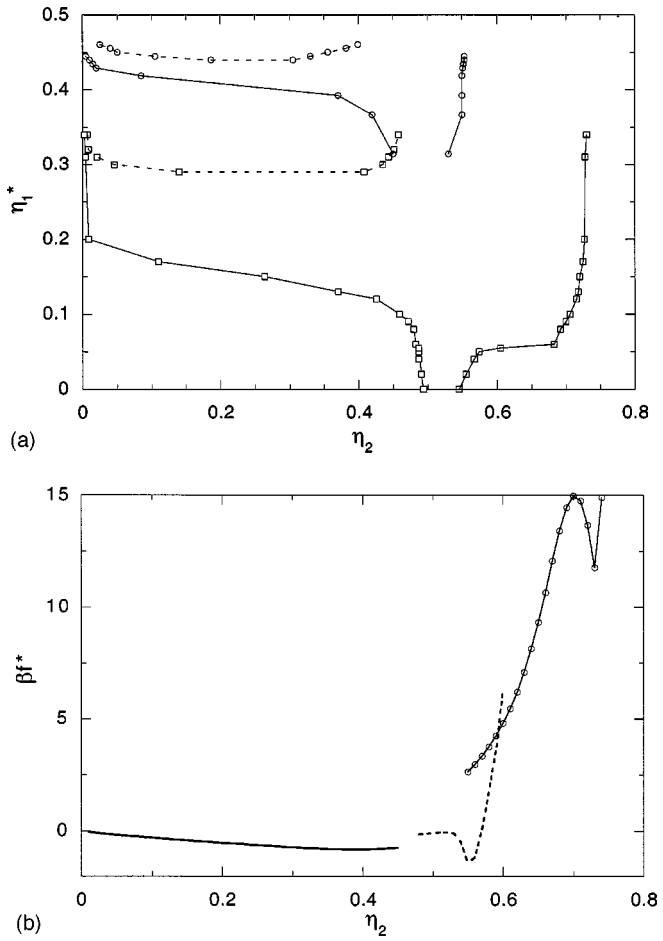

FIG. 8. (a) Influence of the solvent-solvent and solute-solvent attractions on the phase boundaries in the η_1^*-η_2 representation. Size ratio $R=10$. Squares: pure hard sphere mixture, Monte Carlo data [19]; circles: binary mixture with LJ solvent-solvent interaction ($\varepsilon_{11}^*=0.5$) and Yukawa solute-solvent attraction ($\varepsilon_{12}^*=8$, $\kappa=2.5$) RHNC-VPT. Full curves: F-S, dashed curves: F-F. (b) Reduced free energy in the RHNC-VPT [same potential as in (a), $\eta_1^*=0.419$]. Fluid branch (full curve): RHNC. Solid branch: dashed line: full VPT (with σ^{opt}); full curve with circles: PT (diameter fixed to d_2).

no longer possible. This shows that the large widening of the F-S domain discussed in Ref. [19] is likely to be specific to mixtures of pure hard spheres.

V. CONCLUSION

To summarize this work, we may say that the positive comparison of the RHNC-VPT method with simulation data for highly asymmetric mixtures of hard spheres allows us to explore other physical systems that are difficult to study for the moment entirely by simulation. In this work, a very limited sample of such a system has actually been investigated but the results show that when attractions are considered, the pattern is clearly different from that pertaining to pure hard spheres. The most important result is perhaps that such attractions favor the existence of a dense fluid of solute particles, in an equally dense suspending medium. This provides a natural explanation of the observed stable fluid phases of many real colloidal suspensions and confirms the trends deduced from previous structural studies. On the other hand, and given then the variety of effective potentials that can be generated by changing the parameters of the solute-solvent and solvent-solvent attractions, one can easily imagine that an appropriate combination of these interactions will lead to an effective potential for which the fluid-fluid transition can be more stable than the fluid-solid line, and vice versa. However, and besides the amount of numerical work required by such a systematics, further progress in the consistent treatment of both the fluid and the solid is necessary to firmly establish the role of the various attractions in the phase diagram. More extensive simulations of the true mixture are also required for assessing the validity of the effective one-component description. Work on these aspects is currently in progress.

ACKNOWLEDGMENTS

We are indebted to T. Biben for sending us the simulation data required to plot Fig. 1(a). Our special thanks go to M. Dijkstra, R. van Roij, and R. Evans who provided us with a set of partly unpublished simulation results for the free energy.

APPENDIX

The RHNC free energy per particle is given by [51]

$$\beta\frac{A}{N}=\beta\frac{A_1}{N}+\beta\frac{A_2}{N}+\beta\frac{A_3^0}{N}+\beta\frac{\Delta A_3}{N},$$

where

$$\beta\frac{A_1}{N}=-\tfrac{1}{2}\rho\int d\vec{r}\{\tfrac{1}{2}h^2(r)+h(r)-g(r)\ln[g(r)\exp(\beta\phi(r)]\},$$

$$\beta\frac{A_2}{N}=-\frac{1}{2\rho}\int\frac{d\vec{k}}{(2\pi)^3}\{\ln[1+\rho\tilde{h}(k)]-\rho\tilde{h}(k)\},$$

$$\beta\frac{\Delta A_3}{N}=-\frac{1}{2}\rho\int d\vec{r}\int_0^1 d\lambda\, B(r;\lambda)\frac{\partial}{\partial\lambda}g(r;\lambda),$$

$$\beta\frac{A_3^0}{N}=\beta\frac{A_0}{N}-\beta\frac{A_1^0}{N}-\beta\frac{A_2^0}{N},$$

and where $\beta A_1^0/N$ and $\beta A_2^0/N$ are defined as $\beta A_1/N$ and $\beta A_2/N$ with $h(r)$, $g(r)$, and $\phi(r)$ replaced by the corresponding quantities in the reference system, $\beta A_0/N$ being the free energy per particle of the hard sphere reference system. This expression of $\beta A/N$ can be further simplified by using the RHNC closure before numerical evaluation. $\beta A_0/N$ was computed from Erpenbeck and Wood's [78] parametrization of the hard sphere equation of state to remain consistent with the parametrization of $B_0(r)$ of Refs. [55,56] (the Verlet-Weis correction must be computed with the same parametrization [52]). Notice that these references contain misprints (the correct coefficient of η^3 in the numerator of Eq. (7) in [55] reads $-0.343\,029\,8$) (see also [79]). This has a small but sizable influence on the value of $\beta A_0/N$ (this differs from the expression given in Ref. [52]).

[1] S. Asakura and F. Oosawa, J. Chem. Phys. **22**, 1255 (1954).
[2] A. Vrij, Pure Appl. Chem. **48**, 471 (1976).
[3] T. Biben and J. P. Hansen, Phys. Rev. Lett. **66**, 2215 (1991); J. Phys.: Condens. Matter **3**, 65 (1991).
[4] J. L. Lebowitz and S. Rowlinson, Phys. Rev. **41**, 133 (1964).
[5] C. Caccamo and G. Pellicane, Physica A **235**, 149 (1997); C. Caccamo, G. Pellicane, and E. Enciso, Phys. Rev. E **56**, 6954 (1997).
[6] Y. Rosenfeld, Phys. Rev. Lett. **72**, 3831 (1994); J. Phys. Chem. **99**, 2857 (1995).
[7] Y. Martinez-Raton and J. Cuesta, Phys. Rev. E **58**, 4080 (1998).
[8] F. Saija, P. V. Giaquinta, and S. Prestipino Giaritta, J. Phys.: Condens. Matter **6**, 9853 (1994); F. Saija and P. V. Giaquinta, *ibid.* **8**, 8137 (1996).
[9] H. N. W. Lekkerkerker and A. Stroobants, Physica A **195**, 387 (1993); H. N. W. Lekkerkerker, W. C. K. Poon, N. Pusey, A. Stroobants, and P. B. Warren, Europhys. Lett. **20**, 559 (1992).
[10] S. Amokrane and C. Regnaut, Phys. Rev. E **3**, 1990 (1996).
[11] D. Henderson, D. Boda, K. Y. Chan, and D. T. Wasan, Mol. Phys. **95**, 131 (1998).
[12] A. Santos, S. B. Yuste, and M. Lopez De Haro, Mol. Phys. **96**, 1 (1999).
[13] E. Enciso, N. G. Almarza, D. S. Calzas, and M. A. Gonzalez, Mol. Phys. **92**, 173 (1997).
[14] T. Coussaert and M. Baus, J. Chem. Phys. **109**, 6012 (1998).
[15] R. J. Wheatley, F. Saija, and P. V. Giaquinta, Mol. Phys. **94**, 877 (1998).
[16] G. Jackson, J. S. Rowlinson, and F. van Swol, J. Phys. Chem. **91**, 4907 (1987).
[17] P. Bladon, T. Biben, and D. Frenkel, J. Phys.: Condens. Matter **8**, 10 799 (1996).
[18] A. Buhot and W. Krauth, Phys. Rev. Lett. **81**, 378 (1998).
[19] M. Dijkstra, R. van Roij, and R. Evans, Phys. Rev. Lett. **81**, 268 (1998); **82**, 117 (1999); Phys. Rev. E **59**, 5744 (1999).
[20] L. Lue and L. V. Woodcock, Mol. Phys. **96**, 1435 (1999).
[21] N. G. Almarza and E. Enciso, Phys. Rev. E **59**, 4426 (1999).
[22] S. Sanyal, N. Easwar, R. Ramaswamy, and A. K. Sood, Europhys. Lett. **18**, 107 (1992).
[23] J. S. van Duijneveldt, A. W. Heinen, and H. N. W. Lekkerkerker, Europhys. Lett. **21**, 369 (1993).
[24] P. D. Kaplan, J. L. Rouke, A. G. Yodh, and D. J. Pine, Phys. Rev. Lett. **72**, 2215 (1994); A. D. Dinsmore, A. G. Yodh, and D. J. Pine, Phys. Rev. E **52**, 4045 (1995).
[25] H. N. W. Lekkerkerker, J. K. G. Dhont, H. Verduin, C. Smits, and J. S. van Duijneveldt, Physica A **213**, 18 (1995).
[26] C. G. de Kruif, W. J. Briels, R. P. May, and A. Vrij, Langmuir **4**, 668 (1988); C. G. de Kruif, P. W. Rouw, W. J. Briels, M. H. G. Duits, A. Vrij, and R. P. May, *ibid.* **5**, 422 (1989).
[27] M. C. Grant and W. B. Russel, Phys. Rev. E **47**, 2606 (1993).
[28] C. Robertus, J. G. H. Joosten, and Y. K. Levine, Phys. Rev. A **42**, 4820 (1990); J. Chem. Phys. **93**, 7293 (1990).
[29] C. Boned, J. Peyrelasse, and Z. Saïdi, Phys. Rev. E **47**, 468 (1993).
[30] S. H. Chen, J. Rouch, F. Sciortino, and P. Tartaglia, J. Phys.: Condens. Matter **6**, 10855 (1994).
[31] G. Cassin, J. P. Badiali, and M. P. Pileni, J. Phys. Chem. **99**, 12941 (1995).
[32] X. An, J. Chen, Y. Huang, and W. Shen, J. Colloid Interface Sci. **203**, 140 (1998).
[33] S. Brunetti, D. Roux, A. M. Bellocq, G. Fourche, and P. Bothorel, J. Phys. Chem. **87**, 1028 (1983).
[34] L. M. M. Nazario, T. A. Hatton, and J. P. S. G. Crespo, Langmuir **12**, 6326 (1996).
[35] R. J. Baxter, J. Chem. Phys. **49**, 2770 (1968).
[36] C. Robertus, W. H. Philipse, J. G. H. Joosten, and Y. K. Levine, J. Chem. Phys. **90**, 4482 (1989).
[37] M. H. G. M. Penders and A. Vrij, Physica A **173**, 532 (1991); Prog. Colloid Polym. Sci. **88**, 1 (1992).
[38] C. Regnaut, S. Amokrane, and Y. Heno, J. Chem. Phys. **102**, 6230 (1995); S. Amokrane and C. Regnaut, *ibid.* **106**, 376 (1997).
[39] E. Dickinson, J. Chem. Soc., Faraday Trans. **91**, 4413 (1995).
[40] A. Jamnik, J. Chem. Phys. **105**, 10511 (1996).
[41] M. Kinoshita, S. Iba, and M. Harada, J. Chem. Phys. **105**, 2497 (1996).
[42] M. Kinoshita, Mol. Phys. **94**, 485 (1998).
[43] S. Amokrane, J. Chem. Phys. **108**, 7459 (1998).
[44] J. G. Malherbe and S. Amokrane, Mol. Phys. **97**, 677 (1999).
[45] P. Attard and G. N. Patey, J. Chem. Phys. **92**, 4970 (1990).
[46] T. L. Hill, *Statistical Mechanics* (Dover, New York, 1987).
[47] P. Attard, J. Chem. Phys. **91**, 3083 (1989).
[48] A. Malijevski, R. Pospisil, W. R. Smith, and S. Labik, Mol. Phys. **72**, 199 (1991).
[49] F. Lado, Phys. Rev. A **8**, 2548 (1973).
[50] F. Lado, Phys. Lett. **89A**, 196 (1982).
[51] F. Lado, S. M. Foiles, and N. W. Ashcroft, Phys. Rev. A **4**, 2374 (1983).
[52] E. Lomba, Mol. Phys. **68**, 87 (1989).
[53] E. Lomba and N. G. Almarza, J. Chem. Phys. **100**, 8367 (1994).
[54] S. Labik, A. Malijevski, and P. Vonka, Mol. Phys. **56**, 709 (1985).
[55] A. Malijevski and S. Labik, Mol. Phys. **60**, 663 (1987).
[56] S. Labik and A. Malijevski, Mol. Phys. **67**, 431 (1989).
[57] L. Verlet and J. J. Weis, Phys. Rev. A **5**, 939 (1972).
[58] M. Kinoshita and M. Harada, Mol. Phys. **65**, 599 (1988).
[59] Y. Rosenfeld, Phys. Rev. A **29**, 2877 (1984).
[60] Y. Rosenfeld and N. W. Ashcroft, Phys. Rev. A **20**, 1208 (1979).
[61] J. P. Hansen and I. R. Mc Donald, *Theory of Simple Liquids* (Academic, New York, 1986).
[62] J. G. Malherbe (private communication).
[63] A. G. Schlijper, M. M. Telo da Gama, and P. G. Ferreira, J. Chem. Phys. **98**, 1534 (1993); P. G. Ferreira, R. L. Carvalho, M. M. Telo da Gama, and A. G. Schlijper, *ibid.* **101**, 594 (1994).
[64] L. Belloni, J. Chem. Phys. **98**, 8080 (1993).
[65] L. F. Rull, C. Vega, and S. Lago, Mol. Phys. **87**, 1235 (1996).
[66] B. Barboy, J. Chem. Phys. **61**, 3194 (1974).
[67] C. Regnaut, J. Clement-Cottuz, and S. Amokrane (unpublished).
[68] P. V. Giaquinta and G. Giunta, Physica A **187**, 145 (1992).
[69] J. F. Lutsko and M. Baus, Phys. Rev. A **41**, 6647 (1990).
[70] M. Hasegawa and K. Ohno, J. Phys.: Condens. Matter **9**, 3361 (1997).
[71] M. Hasegawa, J. Chem. Phys. **108**, 208 (1998).
[72] A. R. Denton and H. Löwen, J. Phys.: Condens. Matter **9**, 8907 (1997).
[73] Y. Rosenfeld, J. Chem. Phys. **98**, 8126 (1993).
[74] A. A. Louis, R. Finken, and J. P. Hansen, Phys. Rev. E **61**, 1028 (2000).

[75] R. Garibay-Alonso, J. M. Mendez Alcaraz, and R. Klein, Physica A **235**, 159 (1997).
[76] M. H. Hagen and D. Frenkel, J. Chem. Phys. **101**, 4096 (1994).
[77] C. Rascon, G. Navascues, and L. Mederos, Phys. Rev. B **51**, 1499 (1995).
[78] J. J. Erpenbeck and W. W. Wood, J. Stat. Phys. **35**, 321 (1984).
[79] S. Rast, P. H. Fries, and H. Krienke, Mol. Phys. **96**, 1543 (1999).